Scattering Simulations in Inhomogenous Volumes for Scanning Near-field Optical Microscopy

Stanley Humphries, Jr.[+]
Field Precision
Albuquerque, New Mexico 87192

Abstract

This paper describes finite-element techniques to simulate scattering of electromagnetic radiation from objects in inhomogeneous solution spaces. The motivation for the work is the development of software to model field interactions at surfaces for scanning near-field optical microscopes. The calculation is performed in a computational anechoic chamber - a finite volume surrounded by an absorbing layer to simulate free space. The volume may consist of any configuration of materials, including lossy dielectrics and ferrites. The first step in the procedure is to find a distribution of element current sources consistent with the absorbing boundaries that generate the desired unperturbed wave solution. The base solution is not limited to simple plane waves. It may consist of any valid electromagnetic disturbance including mixed propagating and evanescent waves. The second step is to introduce one or more scattering objects and to solve finite-element equations for the perturbed fields. One advantage of the approach is that the boundaries need only absorb the scattered field components. Another useful feature for the microscopy calculations is that the method is equally effective for near and far fields. In simulations of small object scattering the absorbing boundary can be at a distance much less than a wavelength.

Scattering Simulations in Inhomogeneous Volumes for Scanning Near-field Optical Microscopy

Stanley Humphries, Jr.[+]
Field Precision
Albuquerque, New Mexico 87192

1. Introduction

The scattering of radiation has provided an impetus for progress in numerical methods for electromagnetism[1-13]. Applications include radar, antenna design and electromagnetic vulnerability. Typical scattering solutions treat objects in free space illuminated by incident plane waves. In contrast, this paper describes methods to handle propagation of radiation in highly inhomogeneous solution spaces with complex unperturbed solutions. The capability is essential for simulations of near-field optical microscopes[14-16]. The goal of these devices is to resolve features on surfaces that are smaller that the wavelength of the illuminating radiation. Figure 1 shows one approach. In Fig. 1*a* a dielectric surface is internally illuminated by a plane wave with wavelength λ incident above the angle of total internal reflection. The evanescent fields outside the dielectric are confined to a distance near the surface comparable to λ. Figure 1*b* shows a schematic view of a sample surface with subwavelength variations of material composition or topography. A metal or dielectric probe close to the surface can couple to the evanescent fields, producing propagating radiation. As the probe moves, the detected far-field signal will vary depending on the probe's proximity to surface features. In this case, the image resolution is determined by the probe's displacement from the surface and the accuracy of small scanning motions. Resolution in the range 10-50 nm is feasible for optical radiation. Numerical simulations are essential to understand how images relate to the features of the surface. The application presents several challenges for scattering theory: inhomogeneous solution volumes, mixtures of propagating and evanescent waves, and complex surface variations.

Solution methods for inhomogeneous volumes are illustrated in this paper with calculations based on a two-dimensional conformal mesh with triangular elements. The techniques have also been tested in a three-dimensional finite-element code on a regular mesh[17]. Section 2 covers the governing equations and the use of termination layers to represent free-space boundaries. Section 3 introduces the method of distributed internal current sources with applications of plane-wave scattering in a free-space region. Here, the currents are chosen to generate the incident (or unperturbed) wave solution *with the effect of the termination layers included*. Combining the source distribution with the material properties of a scattering object leads to the perturbed

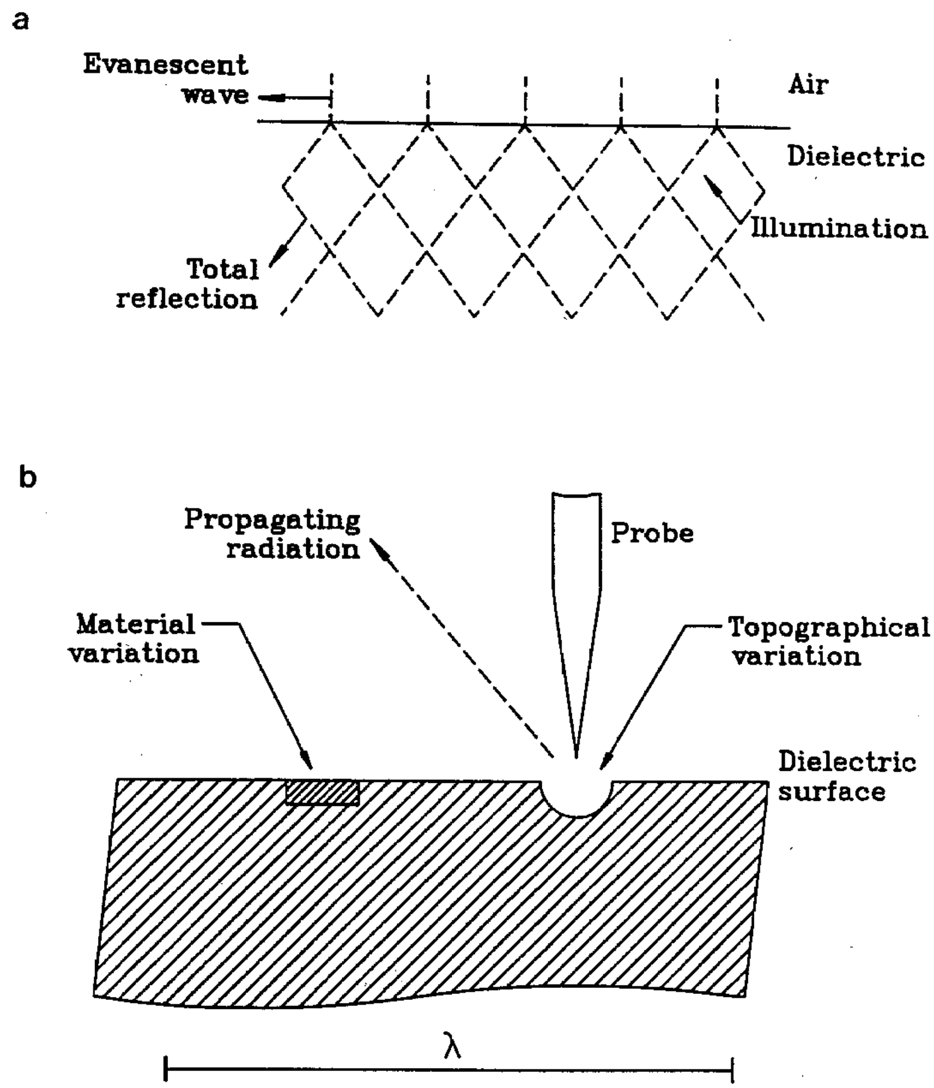

Figure 1. Scanning near-field optical microscopy using internal illumination. a) Illumination of a dielectric surface by a totally-reflected plane wave. b) Detection of sub-wavelength surface features through the interaction of a scanned probe with evanescent fields.

solution. The approach has an advantage similar to scattered field approximation[7]. The termination layer must absorb only the wave components created by the scattering object. Therefore, slightly imperfect absorbing boundaries do not mask the scattered fields. Benchmark calculations are discussed as well as a comparison to more complex methods for representing free-space boundaries. Section 4 covers the extension of the technique to scanning near-field optical microscope simulations. Here, the unperturbed solution consists of standing and evanescent waves adjacent to a dielectric surface (Fig. 1*a*). An important point is that a finite-element program incorporating the distributed source method is inherently a versatile hybrid code. It is easy to incorporate unperturbed wave solutions from any source: analytic or numeric.

2. Governing equations and free-space boundaries

References 17 and 18 review finite-element equations of electromagnetic fields for two-dimensional simplex elements[19]. The examples in this paper are E type solutions in planar geometry. Here, waves with field components E_z, H_x and H_y propagate in the x-y plane. Figure 2 shows an example of a conformal triangular mesh. The solution volume is divided into irregular triangles with edges that lie on the boundaries of material regions. For simplex elements the primary field quantity E_z has values defined at the element vertices (intersection of edges). The subsidiary quantities H_x and H_y are given by

$$H_x = \frac{j}{\mu\omega} \frac{\partial E_z}{\partial y} ,$$
$$H_y = - \frac{j}{\mu\omega} \frac{\partial E_z}{\partial x} . \qquad \textbf{(1)}$$

Equation 1 implies that H_x and H_y are constant within an element. Each element has a unique material identity with associated values of the dielectric constant ε and magnetic permeability μ. vertices.

Application of the integral form of Maxwell's equations for a constant angular frequency ω around a vertex in the mesh of Fig. 2 leads to the following linear equation for the primary field component:

$$-E_{zk} \sum_i W_i + \sum_i W_i E_{zi} = -E_{zk}\, \omega^2 \sum_i \frac{\varepsilon_i a_i}{3} + \sum_i \frac{J_{zi} a_i}{3} . \qquad \textbf{(2)}$$

The subscript *k* refers to a test vertex and *i* refers to the surrounding vertices and elements. The quantity a_i is the area of an element and J_{zi} is the axial source current density. The coupling coefficients W_i are given by

$$W_i = \frac{1}{2} \left[\frac{\cot\theta_{b,i+1}}{\mu_{i+1}} + \frac{\cot\theta_{a,i}}{\mu_i} \right] . \qquad \textbf{(3)}$$

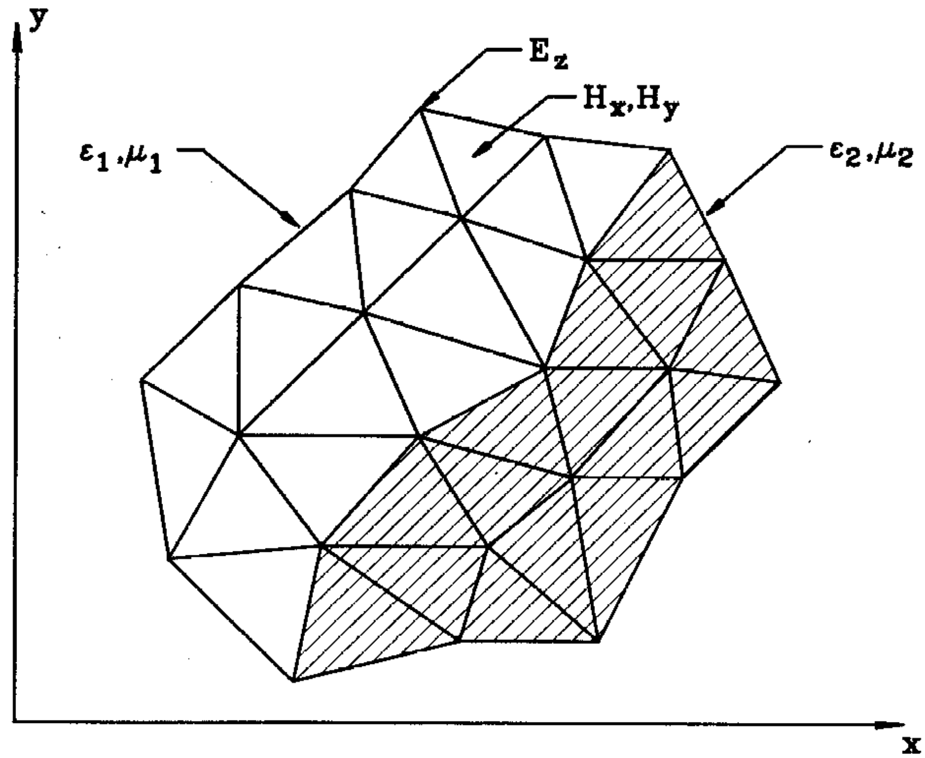

Figure 2. Two-dimensional electromagnetic calculations on a conformal triangular mesh, E-type solutions. Mesh for a planar simulation with E_z defined at the vertices. Material properties and the subsidiary quantities H_x and H_y are associated with elements.

We can write Eq. 2 in the succinct form

$$\sum_i E_{zi} W_i - E_{zk} \left[\sum_i W_i - A_k \right] = S_k \ . \tag{4}$$

where

$$A_k = \omega^2 \sum_i \frac{\varepsilon_i a_i}{3} \ , \tag{5}$$

and

$$S_k = j\omega \sum_i \frac{J_{zi} a_i}{3} \; . \qquad \textbf{(6)}$$

Equation 4 represents a set of coupled linear equations, one for each vertex, that can be solved by direct matrix inversion.

Solutions of Eq. 4 apply to bounded volumes in space. We must specify conditions on the surface of the solution region. Scattering solutions usually require a free-space or outer radiation boundary condition[7,20-27]. Such a boundary is equivalent to a perfect absorber of electromagnetic energy. The termination layer[28,29] is a conceptually simple way to implement the condition. The layer consists of a single layer of absorbing elements adjacent to an unconstrained (open-circuit) boundary. With a proper choice of the complex dielectric constant and magnetic permeability the surface impedance can be matched to the characteristic impedance of the adjacent propagation medium. The process is analogous to a resistive termination of a transmission line. Termination layers work well in scattering calculations where the scattering object is near the center of the solution volume. In this case, scattering waves are almost normally incident on the layer.

In scattering calculations termination layers can be used to define a computational anechoic chamber. A good geometry for two-dimensional calculations is a cylindrical propagation volume centered on the scattering object surrounded by a thin absorbing layer. An incident field of known form (such as a plane wave) drives currents in the object which generate the scattered fields. Drive boundaries with a fixed value of $E_z(t)$ cannot be used inside the chamber to create the incident field because they would reflect scattered fields. Instead, the incident wave must be generated by internal current sources (J_z in Eq. 6). The challenge is to find the proper spatial distribution of J_z to generate an ideal incident wave. One problem is that even small reflections from the termination layer create interference patterns that mask scattered fields of interest.

The frequency-domain calculation shown in Fig. 3 illustrates the difficulty. In the example the goal is to generate an incident plane wave with $\lambda = 1.0$ µm moving 20° with respect to the x-axis inside the homogeneous solution volume. In the simulation the termination layer around the rectangular volume has thickness $\Delta = 0.05$ µm. Following the prescription in Ref. 28, the matched imaginary part of the dielectric constant at normal incidence for the frequency $f = 3.0 \times 10^{14}$ Hz is $\varepsilon'' = -3.178\varepsilon_o$. The value $\varepsilon'' = -3.178\varepsilon_o \sin(70°) = -2.986\varepsilon_o$ is assigned to the left and right layers, while the top and bottom layers have $\varepsilon'' = -3.178\varepsilon_o \sin(20°) = -1.087\varepsilon_o$. A thin current layer on the left generates the plane wave. A harmonic modulation of J_z in the y-direction with wavelength 2.924 µm gives a 20° inclination. Electromagnetic energy moving backward from the layer is absorbed by the adjacent termination layer. Figure 3 shows that the solution generally follows the desired variation but is clearly imperfect. In addition to the effect of the source edge at the bottom, interference produces a 5 per cent vertical modulation of field amplitude.

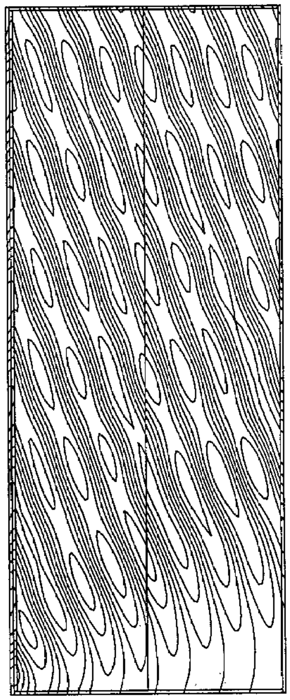

Figure 3. Unsuccessful approach to the generation of a plane wave in an anechoic chamber. Simulation geometry and contours of E_z for the solution. Chamber dimensions: 4.0 µm in x and 10.0 µm in y. Plane wavelength in air with λ = 1.0 µm moving 20° with respect to the x-axis. Solution volume surrounded by a termination layer of thickness Δ = 0.025 µm. Current drive layer on left-hand side.

Section 3. Distributed source method for free-space scattering

It is clear that attempts to guess the correct spatial distribution of J_z lead to noisy solutions of limited use. Instead we shall apply an inverse procedure starting from the desired incident waveform. An analysis of the governing equations leads to J_z distributions that are consistent with the presence of the termination layers. In this paper the procedure will be referred to as the *distributed source method*. This section treats the example of an incident plane wave. Section 4 shows that the method has considerable generality and is consistent with any unperturbed wave solution. To begin, suppose we have an anechoic chamber with a termination layer but no scattering object. The desired field variation for an E-type wave is

$$E_z(x,y) = \xi \exp[-j(k_x x + k_y y)] \ . \qquad \textbf{(7)}$$

If $k_x > 0$ and $k_y = 0$, the expression of Eq. 13 corresponds to a traveling wave with amplitude ξ and wavelength $\lambda = 2\pi/k_x$ moving in the positive x direction. Substitution into Eq. 4 gives

$$S_k = \xi \sum_i \exp[-j(k_x x_i + k_y y_i) \ W_i + \xi \exp[-j(k_x x_k + k_y y_k) \ (\sum_i W_i - A_k) = 0. \qquad \textbf{(8)}$$

Equation 14 defines a source term at each vertex. The coefficients W_i and A_k depend on the material properties of surrounding elements, some of which may be part of the termination layer. If we solve the set of equations represented by Eq. 4 using Eq. 14 for the source terms, the result must satisfy Eq. 13.

The distributed source procedure for a frequency-domain scattering solution consists of the following steps.

1) Set up an anechoic chamber with no scattering object surrounded by termination or symmetry boundaries.

2) Calculate the set of source terms S_k from Eq. 14 using values of W_i and A_k evaluated for the object-free space.

3) Insert the scattering object and recalculate W_i and A_k for all vertices.

4) Solve the set of equations represented by Eq. 4 with the adjusted values of W_i and A_k and the distributed source terms S_k.

5) To analyze the total field solution make a data file of E_{zk} at all vertices. To analyze the scattered field, make a file of the values $E_{zk} - \xi \exp[-j(k_x x_k + k_y y_k)]$ (the total field minus the incident field).

The method has several advantages for finite-element scattering calculations:

• The calculation is efficient in terms of computer resources because the free-space boundaries require only a single layer of elements. In contrast to other approaches[29,30] there is no advantage to multi-element layers.

• There are no limits on the size of the solution volume compared to the wavelength. The method is equally effective for near-field and far-field analyses.

• Because the termination boundaries absorb only the fields scattered from the object, the effects of small reflections are minimized.

• Finite-element calculations using distributed sources are well-suited to scattering objects with complex geometries. It is easy to assign values of complex ε and μ to individual elements to produce structures with graded or mixed properties.

To illustrate the method, consider an extreme example where the scattering object completely changes the nature of the incident wave solution. Figure 4*a* shows the geometry. A one-dimensional vacuum region with length 1.0 m has symmetry boundaries at the top and bottom and termination layers with thickness $\Delta = 0.01$ m at the left and right. The unperturbed solution is a traveling wave with unity amplitude and $\lambda = 0.5$ m incident from the left-hand side. The scattering

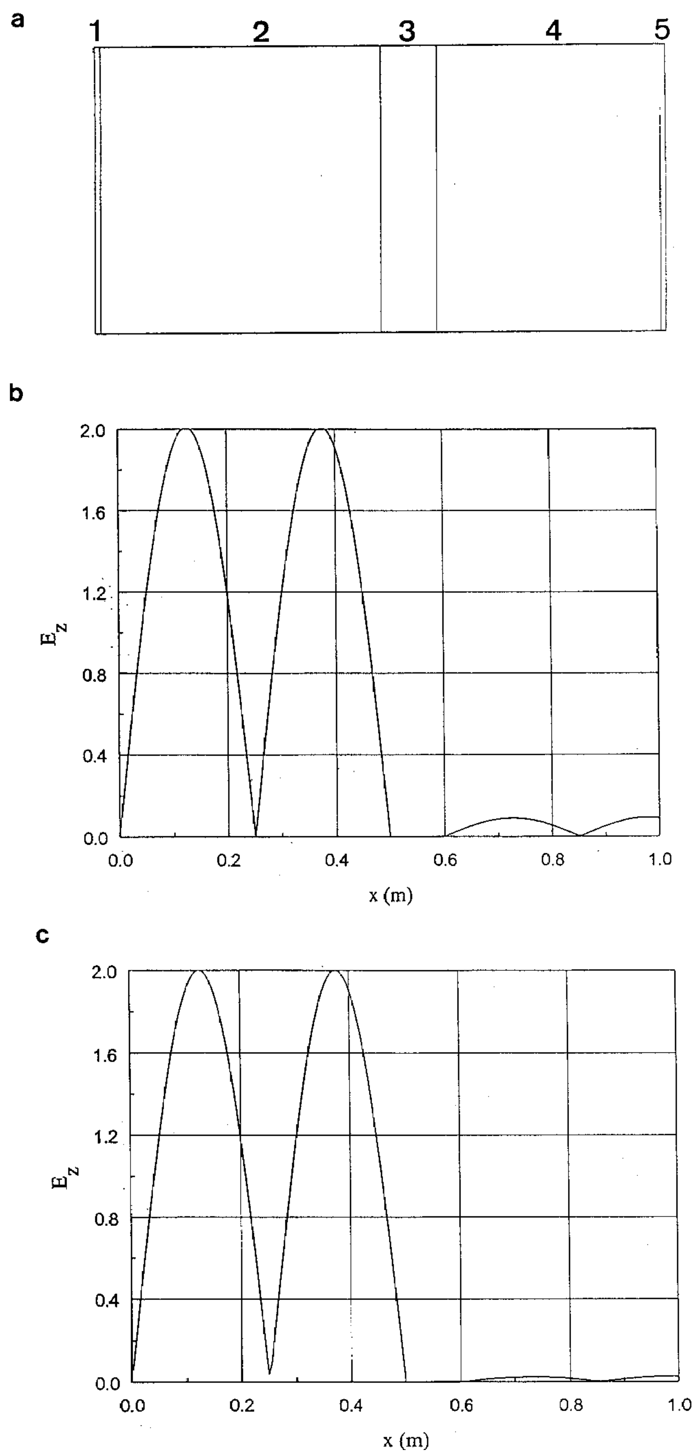

Figure 4. Benchmark test of one-dimensional wave propagation with a large scattering object. a) Solution geometry. The volume has length 1.0 m in x and 0.5 m in y. Radiation: f = 6.0 x 10^8 Hz, λ = 0.5 m. Top and bottom boundaries; open-circuit. Region 1: Upstream absorber. Region 2:

Air. Region 3: Scattering object: air for the unperturbed solution, perfect conductor for the modified solution. Region 4: Air. Region 5. Downstream absorber. b) Plot of |Ez| along x with the metal object in place for a termination layer thickness $\Delta = 0.01$. c) Plot of |Ez| along x with the metal object in place for a termination layer thickness $\Delta = 0.0025$.

object is a metal plate that divides the solution volume. The solution with the object in place should be a standing wave with amplitude 2.0 and period $\lambda/2$ in the upstream region and zero field downstream. The unperturbed solution and source terms are computed with the electric properties of all elements in internal regions set to ε_o and μ_o. To represent the metal plate the material characteristics in the object region are changed to $\varepsilon = 10^{-12}\varepsilon_o$ and $\mu = 10^{12}\mu_o$. This choice preserves the speed of light in the medium while reducing the characteristic impedance close to zero.

Figure 4*b* shows a plot of field amplitude with the metal plate in place. The results are close to the expected behavior. The standing wave on the upstream side has amplitude close to twice that of the incident traveling wave and there is a high degree of field cancellation on the downstream side. The residual field in this region is a standing wave that results from a small reflected component from the absorbing boundary. Complete field cancellation occurs only if the scattered wave amplitude exactly equals that of the incident wave. For a comparison, Ref. 28 shows that the field reflection coefficient for radiation of wavelength λ normally incident on a termination layer of thickness Δ is about 5 per cent for $\lambda/\Delta = 50$. Reflection of the backward-going wave from the metal object surface should create a standing wave with a peak amplitude equal to about 10 per cent of the incident wave amplitude. This figure is consistent with the peak amplitude of 8.7 per cent in Fig. 4*b*. We can improve the results of the frequency-domain calculation by reducing the width of the termination layer (Ref). Figure 4*c* plots the wave amplitude for a layer thickness of $\Delta = 0.0025$ m. The residual field amplitude drops to 2.3 per cent, consistent with the prediction of Ref. 28.

To illustrate two-dimensional solutions we will compare results to the advanced hybrid model calculations of Ref. 31. The authors' goal was to implement nearby absorbing boundaries to simulate wave scattering from objects in free space. The calculation used second-order elements and the Mei method [Ref. 27] to define boundary currents that represent perfect absorbers. Figure 5 shows a difficult problem, scattering from a reentrant object. Plane waves with $\lambda = 10$ m are incident from the left on the object (Fig. 5*a*). The radius of the anechoic chamber is 12.5 m with a symmetry boundary on the bottom. The plot of Fig. 5*b* is a comparison of current density moving along the object surface starting from the midpoint of the front face. The distributed source result is the solid line, the Mei boundary calculation from Ref. 31 is shown as a dashed line while the dotted line represents results from a boundary-element calculation. The Mei calculation failed in this example, and the plotted results are extrapolations from an artificial object boundary. The distributed source calculation is in good agreement with the boundary-element treatment, with better resolution of the current discontinuity on the outer edge of the object and the field enhancement on the downstream tip.

a

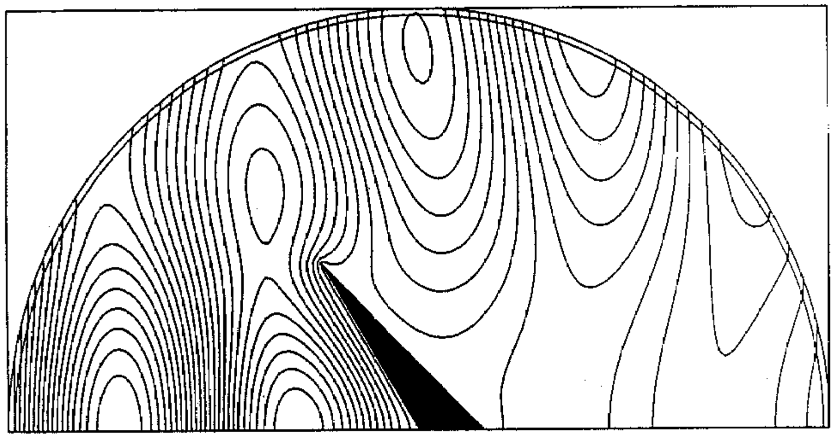

b

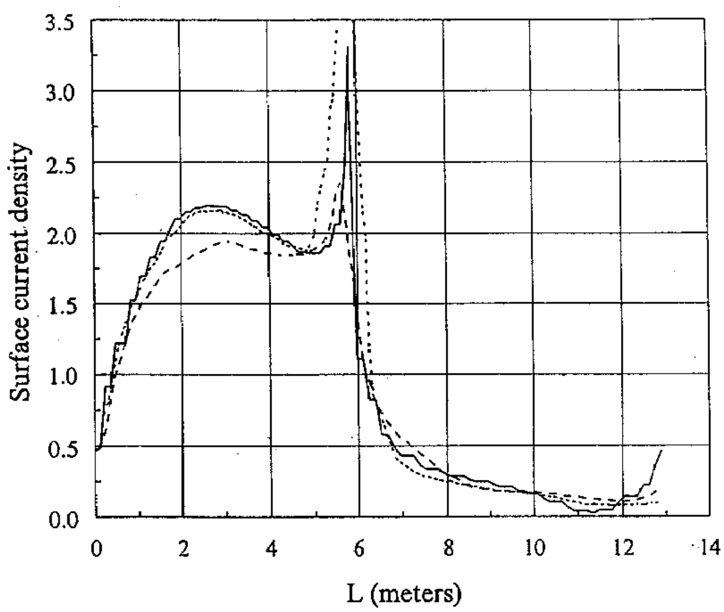

Figure 5. Plane wave scattering from a reentrant metal object. a) Calculation geometry. The solution volume is a half-cylinder of radius 12.5 m with a reflection symmetry boundary along the bottom. A plane wave with λ = 10 m is incident from the left hand side. b) Plot of induced current density on the object as a function of distance from the midpoint of the front face. Solid line: distributed source prediction. Dashed line: result from Ref. 31 using the Mei boundary method. Dotted line: Results from Ref. 31 using a boundary-element model.

4. Distributed source method for inhomogeneous media

This section discusses calculations for inhomogeneous scattering volumes that are difficult to resolve with conventional methods. These calculations are essential for simulations of scanning near-field optical microscopes where phenomena of interest take place less than one wavelength from surfaces. To begin, consider an example that can be directly compared to analytic theory: the quarter-wave transformer. The geometry is similar to that of Figure 4*a*. Waves propagate in the x-direction. There are symmetry boundaries at the top and bottom. Region 2 (-0.5 m to 0.0 m) represents vacuum ($\varepsilon_2 = \varepsilon_o$) with characteristic impedance Z_2 = 377.3 Ω. Region 1 is an absorber with a matched conductivity. On the right-hand side, Region 4 (0.5 m to 1.0 m) is a dielectric with $\varepsilon_4 = 4.0\varepsilon_o$ and Z_4 = 188.7 Ω. For the unperturbed solution Region 3 (0.0 m to 0.5 m) is a dielectric with $\varepsilon_3 = 4.0\varepsilon_o$. In this case, the incident wave should partially reflect at the dielectric discontinuity at x = 0.0. For the scattered wave solution the central region is assigned a dielectric constant $\varepsilon_3 = 2.0\varepsilon_o$. For the choice of frequency f = 101.6 MHz the system is a quarter wave transformer. In this case, the incident traveling wave from the left-hand side should be transformed to a traveling wave with no reflection[32].

This calculation requires a more complex unperturbed solution consisting of incident, reflected and transmitted waves. Following Ref. 29, if the incident wave has electric field amplitude 1.0000 V/m, then the amplitude of the reflected wave is -0.3333 V/m and the transmitted wave is 0.6667 V/m. Multiple plane wave components with correct phase and amplitude are used in Eq. 14 to calculate the source terms. Figure 6 shows plots of the amplitude of E_z as a function of position from the interference of incident and reflected waves. The constant amplitude in the dielectric (0.00 to 1.00 m) marks a pure traveling wave. The variation of Curve B is close to that of an ideal quarter wave transformer solution. The constant amplitude of 1.0 in the vacuum indicates that there is no reflected wave. The traveling wave on the right-hand side is consistent with total energy transfer through the transition. The amplitude is close to the theoretical prediction of $(Z_4/Z_2)^{1/2} = 0.707$. Note that there are mixed standing and traveling waves in the transformer region (0.00 to 0.50 m).

The following set of examples illustrates applications to scanning near-field optical microscopy. The unperturbed solution corresponds to an inhomogeneous volume with propagating and evanescent waves. The goal is to investigate the near-field effects of probes and geometric irregularities on radiation near a dielectric surface with total internal illumination (Fig. 1). The unperturbed solution consists of incident wave, totally-reflected waves and evanescent waves propagating parallel to the surface. Figure 7*a* shows the calculation geometry. The solution region with dimensions 2 μm × 2 μm is surrounding by a termination layer of thickness 0.025 μm. The left-hand side is a dielectric with $\varepsilon_r = 2.0$. A plane wave is incident from the left at 50°, above the critical angle of 45°. The frequency f = 4.243 x 10^{14} Hz gives λ = 0.500 μm in the dielectric and λ = 0.707 μm in vacuum. The amplitudes and wave numbers of the incident, reflected, and evanescent waves were calculated from Ref. 33. Figure 7*b* shows contours of E_z for the unperturbed solution.

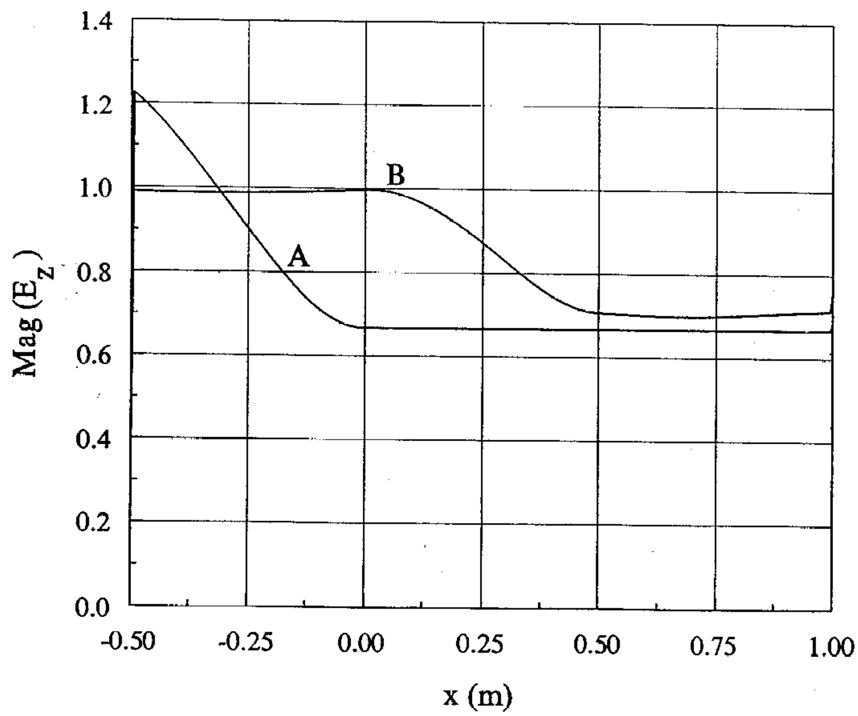

Figure 6. Plot of $|E_z|$ for a quarter wave transformer solution. The upstream vacuum propagation region ($\varepsilon = \varepsilon_o$) extends from -0.50 to 0.00 m. The downstream region has $\varepsilon = 4.0\varepsilon_o$ and extends from 0.5 to 1.0 m. The object (0.0 to 0.5 m) has $\varepsilon = 4.0\varepsilon_o$ for the unperturbed solution and $\varepsilon = 2.0\varepsilon_o$ for the modified solution. A traveling wave with frequency 101.6 MHz is incident from the upstream boundary. Curve A: Unperturbed solution. Curve B: Modified solution.

We can create interesting solutions by adding perturbing objects. The first example, illustrated in Fig. 8*a*, is a broad extension of the dielectric surface with thickness 0.4λ. The figure shows the total field determined by the distributed source method. Introduction of the object radically alters the nature of the local fields. The standing wave solution extends to the new surface and the evanescent waves propagate around the extension. A second example (shown in Figs. 8*b* and 8*c*) is a metal probe in vacuum a distance 0.1λ from the surface. The probe modifies the total fields (Fig. 8*b*) by excluding magnetic fields from its volume. Currents excited in the probe by the evanescent fields generate propagating radiation in the air region. Figure 8*c* shows the scattered fields created by the probe.

The distributed source method is not limited to unperturbed solutions composed of plane waves. The geometry of the solution volume can have any degree of complexity and the base solution can be any valid field consistent with the geometry. The source of the unperturbed solution can be analytic formulas or numerical results from another type of code. There are only two requirements to set up a distributed-source finite-element calculation: 1) identification of the

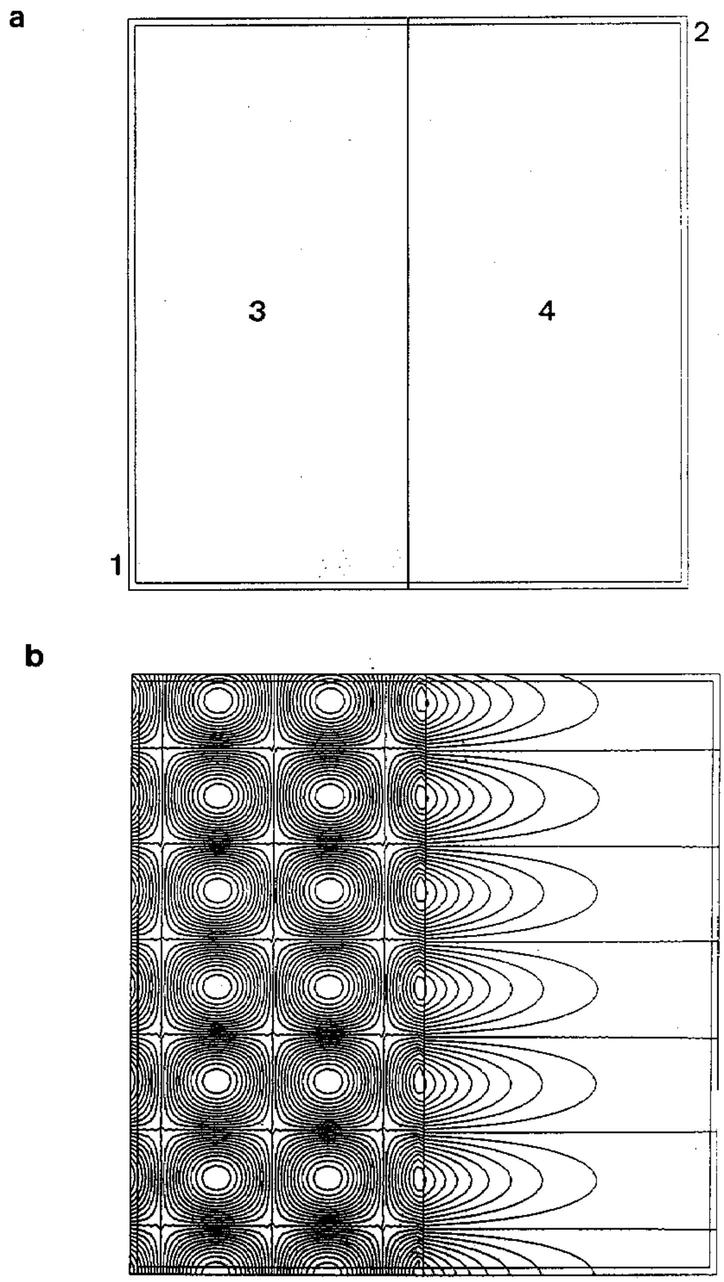

Figure 7. Simulation of total internal reflection and evanescent fields near a dielectric surface. a) Geometry. The solution region with length 2 µm in x and y is surrounding by a termination layer of thickness 0.025 µm. Region 1: Termination layer matched to the characteristic impedance of Region 3. Region 2: Termination layer matched to the characteristic impedance of Region 4. Region 3: Dielectric, $\varepsilon = 2.0\varepsilon o$. Region 4: Air. b) Contours of E_z for a plane wave at frequency 4.243×10^{14} Hz incident from the left-hand side at 50°.

a

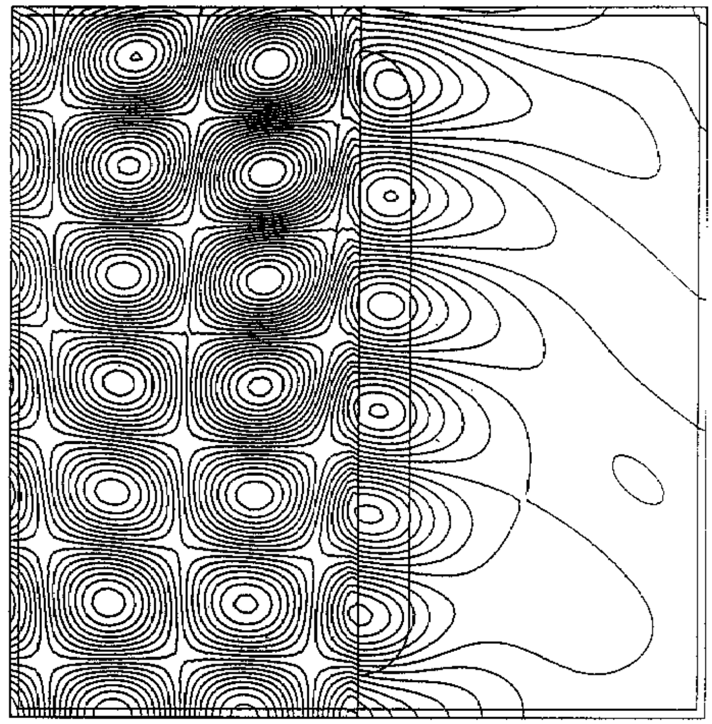

b

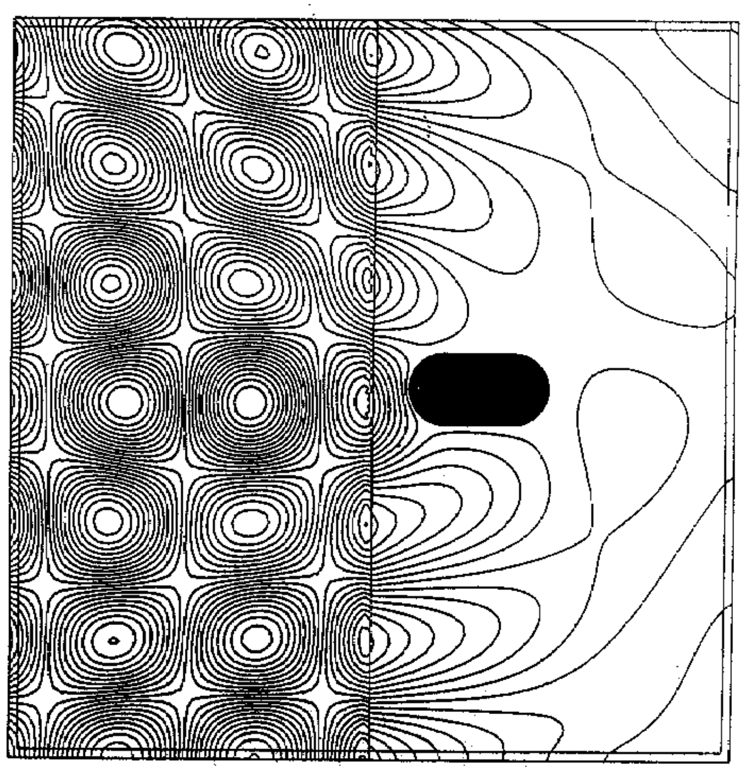

c

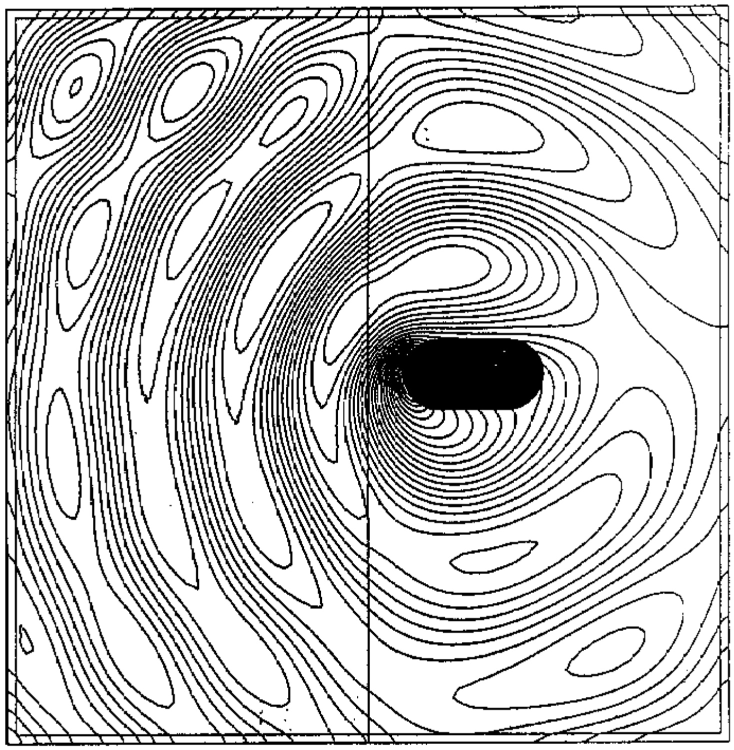

Figure 8. Modifications of the solution of Fig. 7 by scattering objects, contours of E_z. a) Shaped surface extension of thickness 0.14 µm, total fields. b) Metal probe 0.1 µm from the surface, total fields. c) Metal probe 0.1 µm from the surface, scattered fields.

electrical properties of the elements and 2) a method to interpolate field values at vertex locations to determine the sources S_k. The implication is that a finite-element code with distributed-source capabilities has built-in hybrid capabilities. The strategy is to map a subset of any valid electromagnetic solution to an appropriate computational anechoic chamber, add geometric or material perturbations, and then proceed to a solution for the modified fields using the methods described in Sects. 2, 3 and 4.

Acknowledgments

This work was supported by the National Institute of Science and Technology under SBIR Contract 50-DKNB-7-90117. I would like to thank Garnett Bryant for suggesting the demonstration calculations of Figs. 7 and 8.

References

+ Alternate address: Department of Electrical and Computer Engineering, University of New Mexico, Albuquerque, New Mexico 87131.

1. K.J. Binns and P.J. Lawrence, **The Analytic and Numerical Solution of Electric and Magnetic Fields** (Wiley, New York, 1992).
2. M.V. Chari and P.P. Silvester, P.P. (eds.), **Finite Elements for Electrical and Magnetic Field Problems** (Wiley, New York, 1980).
3. Z.J. Csendes (ed.), **Computational Electromagnetism** (North-Holland, New York, 1986).
4. Y. Eikichi (ed.), **Analysis Methods for Electromagnetic Wave Problems** (Artech House, Norwood, Massachusetts, 1990).
5. R.C. Hansen (ed.), **Moment Methods in Antennas and Scattering** (Artech House, Norwood, Massachusetts, 1990).
6. J. Jin, **The Finite-element Method in Electromagnetics** (Wiley, New York, 1993).
7. K.S. Kunz and R.J. Luebbers, **The Finite-difference Time-domain Method for Electromagnetics** (CRC Press, Boca Raton, Florida, 1993), Chap. 18.
8. E.K. Miller, L. Medgyesi-Mitschang and E.H. Newman, **Computational Electromagnetics** (IEEE Press, Piscataway, New Jersey, 1992).
9. R. Mittra (ed.), **Computer Techniques for Electromagnetics** (Pergamon Press, Oxford, 1973).
10. M.A. Morgan (ed.), **Finite-element and Finite-difference Methods in Electromagnetic Scattering** (Elsevier, New York, 1990).
11. M.N.O. Sadiku, **Numerical Techniques in Electromagnetics** (CRC Press, Boca Raton, 1992).
12. C.W. Steele, **Numerical Computation of Electric and Magnetic Fields** (Van Nostrand Reinhold, New York, 1987).
13. Strait, B.J., **Applications of Moment Methods to Electromagnetics** (SCEEE Press, St. Cloud, Florida, 1980).
14. D. Courjon and C. Bainier, Rep. Prog. Phys. **57** (1994), 989.
15. U. Dűrig, D.W. Pohl and H. Rohrer, J. Appl. Phys. **59** (1986), 27.
16. E. Betzig, L. Lewis, A . Harootunian, A. Isaacson and E. Kratschmer, Biophys. **49** (1986), 269.
17. S. Humphries, Jr., **Field Solutions on Computers** (CRC Press, Boca Raton, Florida, 1997), Chap. 14.
18. J.L. Warren, et.al., **Reference Manual for the Poisson/Superfish Group of Codes** (Los Alamos National Laboratory, LA-UR-87-126, 1987), Sect. B.13.6.
19. P.E. Allaire, **Basics of the Finite-element Method** (Wm. C. Brown Publishers, Dubuque, Iowa, 1985), Chap. 3.
20. A. Bayliss and E. Turkel, SIAM J. Appl. Math. **42**, 430 (1982)
21. B. Engquist and A Majda, Math. Comp. **31**, 629 (1977).
22. R.L. Higdon, Math. Comp. **47**, 437 (1986).
23. O.M. Ramahi, A. Kheber and R. Mittra, IEEE Trans. Antennas and Propagation **AP-39**, 350 (1991).
24. G.A. Kriegsmann, A. Taflove and K.R. Umashankar, IEEE Trans. Antennas and Propagation

AP-35 (1987).
25. Berenger, J. Comp. Phys. **114**, 185 (1994).
26. G. Mur, IEEE Trans. Electromagnetic Compatibility **23**, 1073 (1981).
27. M.D. Prouty, K.K. Mei, S.E. Scwarz and R. Pous, IEEE Guided Wave Lett. **3**, 302 (1993).
28. S. Humphries, Jr., op.cit., Sects, 13.1, 13.3 and 14.2.
29. An early conducting layer method was described in A. Taflove and M. Brodwin, IEEE Trans. MTT **23**, 623 (1975). The approach involves matching of a multi-element layer at a single frequency.
30. J.F. DeFord, *Investigation of the limitations of perfectly-matched absorber boundaries in antenna application*, in E.C. Michelson (ed.), **Proc. Applied Computational Electromagnetics Conf.** (Naval Postgraduate Shool, Monterrey, California, 1997), 592.
31. Y. Li and Z.J. Cendes, *A modified Mei method for solving scattering problems with the finite-element method* in E.C. Michelson (ed.), **Proc. Applied Computational Electromagnetics Conf.** (Naval Postgraduate Shool, Monterrey, California, 1997), 566.
32. D.K. Cheng, **Field and Wave Electromagnetics** (Addison-Wesley, Reading, Massachusetts, 1992), 406.
33. J.D. Kraus, **Electromagnetics** (McGraw-Hill, New York, 1992), Sect. 13.6.